Notes and correspondence: Rayleigh scattering by hexagonal ice crystals and the interpretation of dual-polarisation radar measurements

C. D. Westbrook*

Department of Meteorology, University of Reading, UK

*Correspondence to: Dr. Chris Westbrook, Department of Meteorology, University of Reading, PO Box 243, Reading, RG6 6BB, UK

Dual-polarisation radar measurements provide valuable information about the shapes and orientations of atmospheric ice particles. For quantitative interpretation of these data in the Rayleigh regime, common practice is to approximate the true ice crystal shape with that of a spheroid. Calculations using the discrete dipole approximation for a wide range of crystal aspect ratios demonstrate that approximating hexagonal plates as spheroids leads to significant errors in the predicted differential reflectivity, by as much as 1.5dB. An empirical modification of the shape factors in Gans's spheroid theory was made using the numerical data. The resulting simple expressions, like Gans's theory, can be applied to crystals in any desired orientation, illuminated by an arbitrarily polarised wave, but are much more accurate for hexagonal particles. Calculations of the scattering from more complex branched and dendritic crystals indicate that these may be accurately modelled using the new expression, but with a reduced permittivity dependent on the volume of ice relative to an enclosing hexagonal prism.

Key Words: microwave scattering, ice crystal, dual-polarisation

Received . . .

Citation: . . .

1. Introduction

Dual polarisation radar is a powerful tool to study ice particles in the atmosphere. Measurements of differential reflectivity, differential phase shift and the copolar cross correlation coefficient are now commonplace on research radars, and are becoming increasingly available on operational weather radars (Illingworth 2003; Ryzhkov *et al.* 2005). Quantitative interpretation of these data require accurate scattering models for the non-spherical shapes of natural ice particles, and this presents a difficulty. For pristine hexagonal crystals such as plates and columns, common practice is to approximate these shapes by spheroids (e.g. Andrič *et al.* 2013, Westbrook *et al.* 2010, Hogan *et al.* 2002, Ryzhkov *et al.* 1998, Bader *et al.* 1987, Hall *et al.* 1984), and apply Gans (1912)'s theory to solve for the scattered field. These pristine hexagonal crystal shapes are rare in cold upper tropospheric cirrus (where polycrystals such as bullet-rosettes typically dominate, see e.g. Heymsfield and Knollenberg 1972), but appear to be quite common in warmer mid-level cloud layers (Westbrook *et al.* 2010; Westbrook and Illingworth 2013). For qualitative interpretation of radar measurements approximating these hexagonal crystals as spheroids is likely to be a reasonable approach. However there is increasing interest in validating microphysical models by forward modelling the associated dual-polarisation radar parameters and comparing these quantitatively against observations (e.g. Andrič *et al.* 2013). This means that the accuracy of the spheroid scattering model for real crystals becomes rather more important.

In this note we will focus exclusively on the Rayleigh limit where the crystals are much smaller than the radar wavelength. This is appropriate for essentially all ice crystals when considering S-band (10cm) radars such as the Chilbolton Advanced Meteorological Radar (Hall *et al.* 1984). Vapour grown ice crystals grow to sizes of a few millimetres at most (e.g. Takahashi *et al.* 1991). It may well also be useful in many cases for shorter wavelengths provided that the particle dimensions are sufficiently small.

A number of previous studies have used the discrete dipole approximation (DDA, Draine and Flatau 1994) or closely related techniques to investigate the scattering properties of hexagonal ice crystals. Many of these have focussed on millimetre cloud radars where the scattering may be outside the Rayleigh regime. O'Brien and Goedecke (1988) computed the scattering from an idealised planar dendritic crystal and a long hexagonal column of maximum dimension 4mm at a wavelength of 1cm, and found that the scattering cross-sections were often significantly different to those of spheroids with the same dimensions. Evans and Vivekanandan (1990) computed scattering properties of distributions of horizontally oriented cylinders and plates at 8, 3.5 and 1.9mm wavelengths and used these to simulate radar parameters and microwave radiative transfer through ice clouds. Liu (2008) performed DDA calculations for hexagonal prisms of 5 different aspect ratios for particles 50μm–1.25cm in maximum dimension, at wavelengths between 2cm and 0.9mm. They also simulated some idealised dendritic shapes. Random orientation of the crystals was assumed however, and hence no dual-polarisation information can be derived from these results.

Schneider and Stephens (1995) used DDA to simulate horizontally oriented hexagonal columns and plates varying from 50μm to 2mm in maximum dimension at wavelengths of 1.4, 3.2 and 8.7mm and compared them to results obtained by assuming the particles were spheroids. A single aspect ratio was simulated for each crystal size. Some of the smaller particles in this study fall within the Rayleigh limit, and Schneider and Stephens (1995)'s results suggest that the errors in the backscatter cross-sections were of order $\sim$10%. However these error estimates only apply to the specific aspect ratios which Schneider and Stephens (1995) considered; in addition they found significant errors in the DDA results themselves, observing an error of order 15% when comparing the backscatter of spheroids computed by DDA in the Rayleigh regime relative to Gans theory. They attributed this to the relatively coarse discretisation of the particle which was used. The increase in computational resources over the past 2 decades mean that much more accurate results are now possible.

In what follows new DDA calculations are presented for hexagonal ice crystals covering a wide range of aspect ratios ranging from long slender hexagonal columns (1:50) to very thin hexagonal plates (100:1). This covers the range of aspect ratios typically seen in nature (Pruppacher and Klett 1997), and as we will see in section 3 the results at the extreme aspect ratios approach an asymptotic limit in any case. By focussing exclusively on the Rayleigh regime, the analysis of this data can be simplified to the estimation of 2 'polarisabilities' for each ice crystal. Once these polarisabilities are known, the differential scattering cross-sections of that ice crystal in any orientation with respect to the incident wave's polarisation, in any scattering direction, and for any given size crystal can be computed immediately. The DDA results are compared to those predicted by Gans (1912)'s spheroid theory, and this allows us to evaluate the errors associated with the spheroid approximation over a much wider range of aspect ratios than has previously been attempted, with a focus on dual-polarisation parameters, in particular the differential reflectivity Z_{DR}.

2. Theory

We begin with a brief review of some relevant scattering theory. In the Rayleigh regime the applied electric field is uniform across the scatterer and the scattering problem is effectively reduced to an electrostatic one (van de Hulst 1957). The ice particle acts as a radiating point dipole in the far field, and the problem is thus simplified to determining the induced dipole moment $\mathbf{p}$ for a given applied electric field $\mathbf{E_0}$. This relationship is determined by the 'polarisability' of the particle $\mathbf{X}$:

$$\mathbf{p} = 4\pi\epsilon_0 \mathbf{X}\mathbf{E_0} \tag{1}$$

where ϵ_0 is the permittivity of free space. Here $\mathbf{X}$ is a symmetric 3×3 tensor containing at most 6 independent elements (Senior 1976). The elements X_{ij} are proportional to the volume of the scattering particle (the units of X_{ij} are [m^3]), and also depend on the shape and permittivity of the particle. The scattered electric field at a point $\mathbf{r}$ is:

$$\mathbf{E_s}(\mathbf{r}) \quad = \quad k^2 \frac{\mathrm{e}^{ikr}}{4\pi\epsilon_0 r} [\hat{\mathbf{r}} \times (\mathbf{p} \times \hat{\mathbf{r}})] \tag{2}$$

where $r = |\mathbf{r}|$. We suppress the harmonic oscillation $\exp(ikct)$ since this constant factor is present in both the applied and scattered fields, and we are ultimately only interested in the amplitude of $\mathbf{E_s}(\mathbf{r})$. Here t is time, c is the speed of light, and the wavenumber $k = 2\pi/\lambda$ where λ is the wavelength of the radar.

In this paper unit vectors are identified with a circumflex: $\hat{\mathbf{r}}$ represents a unit vector in the scattering direction. The factor $[\hat{\mathbf{r}} \times (\mathbf{p} \times \hat{\mathbf{r}})]$ in equation 2 therefore describes the well-known doughnut-shape radiation pattern of a point dipole in the far field and is simply equal to $\mathbf{p}$ in the case where the scattering direction and induced dipole moment are perpendicular, or zero if they are parallel (since an electromagnetic wave must be polarised perpendicular to its direction of propagation).

The radar cross section of a particle may be related to the scattered electric field in an analogous manner to that given by Seliga and Bringi (1976). If our radar transmits a wave of magnitude E_0 and polarisation $\hat{\mathbf{E}}_0 = \mathbf{E}_0/E_0$, then the copolar radar cross section is simply $4\pi r^2 \times |\mathbf{E_s} \cdot \hat{\mathbf{E}}_0|^2/E_0^2$, i.e.:

$$\begin{aligned}\sigma_{\mathrm{co}} &= 4\pi k^4 \left|[\hat{\mathbf{r}} \times (\mathbf{X}\hat{\mathbf{E}}_\mathbf{0}) \times \hat{\mathbf{r}}] \cdot \hat{\mathbf{E}}_0\right|^2 \\ &= 4\pi k^4 \left|(\mathbf{X}\hat{\mathbf{E}}_\mathbf{0}) \cdot \hat{\mathbf{E}}_0\right|^2 \end{aligned} \tag{3}$$

Here we have applied the vector identity $\hat{\mathbf{r}} \times (\mathbf{X}\hat{\mathbf{E}}_\mathbf{0}) \times \hat{\mathbf{r}} = \mathbf{X}\hat{\mathbf{E}}_0 - [\hat{\mathbf{r}} \cdot (\mathbf{X}\hat{\mathbf{E}}_0)]\hat{\mathbf{r}}$, and realised that in the case of backscatter the second term on the right hand side of this identity is orthogonal to $\hat{\mathbf{E}}_0$ and therefore makes no contribution to σ_{co} (Russchenberg 1992; Bringi and Chandrasekar 2001). Analogously, the cross-polar radar cross-section is:

$$\begin{aligned}\sigma_{\mathrm{cross}} &= 4\pi k^4 \left|[\hat{\mathbf{r}} \times (\mathbf{X}\hat{\mathbf{E}}_\mathbf{0}) \times \hat{\mathbf{r}}] \cdot (\hat{\mathbf{E}}_0 \times \hat{\mathbf{r}})\right|^2 \\ &= 4\pi k^4 \left|(\mathbf{X}\hat{\mathbf{E}}_\mathbf{0}) \cdot (\hat{\mathbf{E}}_0 \times \hat{\mathbf{r}})\right|^2 \end{aligned} \tag{4}$$

noting that the unit vector $\hat{\mathbf{E}}_0 \times \hat{\mathbf{r}}$ describes the polarisation of the cross-polar channel since it is orthogonal to both the transmitted polarisation and the direction of propagation.

In summary, once $\mathbf{X}$ is known for a particular shape, then the dipole moments and hence the scattered field for an arbitrary incident polarisation can be computed, and the radar cross-sections for arbitrary transmitted and received polarisations can be predicted. Our aim in what follows therefore is to estimate $\mathbf{X}$ for some shapes relevant to ice crystals in the atmosphere.

There are a number of ways to determine $\mathbf{X}$ for a given shape, but direct analytical results are very difficult for all but the simplest cases. One shape for which this is possible is an ellipsoid (Gans 1912). Let us choose the coordinate system (described by standard cartesian basis vectors $\hat{\mathbf{x}}$, $\hat{\mathbf{y}}$, $\hat{\mathbf{z}}$) such that the principal axes of the ellipsoid lie parallel to them. In this case $\mathbf{X}$ is diagonal and the elements are

$$X_{ii} = \frac{V}{4\pi} \times \frac{\epsilon - 1}{L_i(\epsilon - 1) + 1} \tag{5}$$

where V is the volume of the particle, L_i is a function of the aspect ratio (van de Hulst 1957), and ϵ is the relative permittivity. For a spheroidal particle the situation is simplified further as two of the three elements of $\mathbf{X}$ are now equal. Let us choose the axis of revolution to be aligned with the $\hat{\mathbf{z}}$ axis – in this case the shape factors L_i are:

$$L_z = \frac{1-e^2}{e^2}\left(-1 + \frac{1}{2e}\ln\frac{1+e}{1-e}\right) \tag{6}$$

for prolate (cigar-shaped) particles, while for oblate (pancake-shaped) spheroids, one obtains:

$$L_z = \frac{1+e^2}{e^2}\left(1 - \frac{1}{e}\tan^{-1} e\right) \tag{7}$$

where e is the eccentricity of the spheroid. In both cases the shape factors corresponding to the $\hat{\mathbf{x}}$ and $\hat{\mathbf{y}}$ axis axes are $L_x = L_y = (1 - L_z)/2$.

Seliga and Bringi (1976) considered the case of oblate spheroids (raindrops) oriented so that their long axes were oriented horizontally and their short axis was aligned vertically. For a radar dwelling at zero elevation angle (horizontal incidence), and transmitting horizontally ($\hat{\mathbf{E}}_\mathbf{0} = \hat{\mathbf{x}}$) and vertically ($\hat{\mathbf{E}}_\mathbf{0} = \hat{\mathbf{z}}$) polarised waves the corresponding copolar radar cross-sections $\sigma_{\mathrm{co,h}}$ and $\sigma_{\mathrm{co,v}}$ are simply:

$$\sigma_{\mathrm{co,h}} = 4\pi k^4 |X_{xx}|^2 \tag{8}$$

$$\sigma_{\mathrm{co,v}} = 4\pi k^4 |X_{zz}|^2 \tag{9}$$

recognising that $\mathbf{X}\hat{\mathbf{E}}_0$ is perpendicular to $\hat{\mathbf{r}}$ and parallel to $\hat{\mathbf{E}}_0$ in this particular case. The differential reflectivity $Z_{DR} = \sigma_{\mathrm{co,h}}/\sigma_{\mathrm{co,v}}$ for an oblate particle of a given aspect ratio is then simply:

$$Z_{DR} = \frac{|X_{xx}|^2}{|X_{zz}|^2} \tag{10}$$

Analogous calculations have been performed by Hall *et al.* (1984) and Hogan *et al.* (2002) (amongst others) for oblate spheroid ice crystals to compute Z_{DR} as a function of aspect ratio, and show that 10dB is the maximum possible differential reflectivity from thin plate crystals. Hogan *et al.* (2002) also considered prolate ice spheroids with their long axis lying in the horizontal plane. Here the calculation is a little more complicated since the long ($\hat{\mathbf{z}}$) axis of the crystal may be aligned in an arbitrary direction in the horizontal plane, while the horizontal polarisation vector $\hat{\mathbf{E}}_0$ is fixed. This means that equation 3 must be integrated over all possible ($\hat{\mathbf{z}}$,$\hat{\mathbf{E}}_0$) combinations, leading to the result:

$$Z_{DR} = \frac{3}{8}\frac{|X_{zz}|^2}{|X_{xx}|^2} + \frac{3}{8} + \frac{1}{4}\frac{|X_{zz}|}{|X_{xx}|} \tag{11}$$

Hogan *et al.* (2002) found that the maximum differential reflectivity from thin column crystals was 4dB.

The use of the analytical results (5,6,7) for spheroids to compute the polarimetric properties of ice crystals is very common. However the accuracy of this approximation for hexagonal ice crystals has not been clearly established. In section 3 we will determine the errors involved in this approximation using numerical calculations of $\mathbf{X}$ for hexagonal ice prisms. Following this a simple empirical modification to Gans's theory is proposed to more accurately capture the scattering properties of hexagonal ice crystals.

3. Hexagonal prisms: numerical data and a new empirical formula

For a hexagonal ice crystal no exact solution currently exists for $\mathbf{X}$. However we can obtain some useful information about its form. Senior (1976) has shown that for particles with two perpendicular axes of symmetry (such as an ice crystal with hexagonal symmetry), $\mathbf{X}$ is diagonal, as it is for an ellipsoid. This means we need to determine at most 3 numbers for a given crystal shape, and in what follows we will use numerical solutions for the scattered fields from various crystal shapes to determine a simple approximate formula for $\mathbf{X}$.

3.1. DDA calculations

To determine the 3 polarisability tensor elements for hexagonal ice crystals the DDA method was used. This approach involves discretising the particle into many small volume elements, each of which is represented by a point dipole. Knowing the polarisability of each of these small (cubic) ice volumes allows the scattered field due to each volume element to be determined as a function of the applied electric field and the scattered field from all other volume elements in the particle. This system of equations is then inverted to obtain the electric field at each volume element, and hence the far-field scattering pattern and polarisability tensor elements. Full details of the method are given by Draine and Flatau (1994)*, and provided that the permittivity of the particle is not very strong, and a sufficient number of dipoles is used to represent the shape of the crystal, this approach should provide quite accurate estimates of X_{ii}. The key advantage of this method is its flexibility - the scattering for an arbitrary shape can be calculated, and particles with large aspect ratio can be handled without difficulty. Draine and Flatau (1994) show

*The calculations in this paper were performed using version 6.1 of the DDSCAT package used by Draine and Flatau (1994); repetition of these calculations using version 7.3 (the latest release at the time of writing) gave identical results (RMS fractional difference of 0.1%).

comparisons of the differential scattering cross sections of spherical particles validated against Mie theory for permittivities comparable to ice and the error in the DDA estimates were <3% in the backscatter direction using $\sim 10^4$ dipole elements or more. Zubko *et al.* (2010) has noted that the sphere is one of the most challenging geometries to simulate accurately using DDA. In the calculations for hexagonal prisms below we used between 4×10^5 and 2×10^6 dipole elements; for the branched plate crystals in section 4 memory limitations combined with the open geometry of some of the shapes meant that fewer dipole elements were used, but in all cases this was $> 10^5$. Based on this we expect errors smaller than Draine and Flatau (1994) obtained, which should be more than sufficient for the practical purpose of estimating radar parameters.

Figure 1 illustrates the geometry of the crystals. Right regular hexagonal prisms were constructed. On the basal (hexagonal) faces the sides of the hexagon have length a, and hence the maximum span across the basal facet is $2a$. The span of the crystal along the prism axis is L. The prism axis is oriented along the $\hat{\mathbf{z}}$ direction, while $\hat{\mathbf{x}}$ and $\hat{\mathbf{y}}$ lie in the basal plane. This geometry is fixed for all the simulations, and the DDA calculations are performed 3 times for incident waves polarised parallel to $\hat{\mathbf{x}}$, $\hat{\mathbf{y}}$ and $\hat{\mathbf{z}}$: this is sufficient to determine the 3 non-zero elements of $\mathbf{X}$. The permittivity of the particles was set equal to that of solid ice $\epsilon = 3.15 + i\delta$. Since δ is a very small number ($\sim 5 \times 10^{-4}$ at S-band: Liebe *et al.* 1989) we ignore the resulting imaginary components of the polarisability tensor, and report only the real parts. This is consistent with the negligible attenuation typically produced by non-melting ice particles in the microwave (Atlas and Ludlam 1961). To ensure that the calculations are firmly in the Rayleigh regime the equivalent-volume radius of the ice crystals was set to 10μm which is indeed much smaller than the 10cm wavelength. The specific choice of crystal size is not important since the elements of $\mathbf{X}$ are simply proportional to the volume, and so the results can be simply scaled up or down as desired, and in what follows we will actually report polarisabilities which have been normalised by the volume of the crystal.

The results of these calculations are shown in figure 2 as a function of aspect ratio $w = 2a/L$ ranging from 0.02 (a long slender column) to 100 (a thin plate).The elements of X_{ii} have been normalised by a factor $V/(4\pi)$ and are now dimensionless, depending on the shape and permittivity of the particle alone. Although the author is not aware of any theoretical reason to require it, it is observed numerically that the elements X_{xx} and X_{yy} are essentially identical (within $\approx 1\%$ of each other), and hence only X_{xx} and X_{zz} are reported in figure 2. Also plotted on this figure are the theoretical results for spheroids (equations 5, 6 and 7). Note that this method of comparison implicitly means that we are considering a spheroid with a volume and aspect ratio equal to that of the hexagonal crystal it is intended to represent, and this is logical since $\mathbf{X} \propto V$. Other choices of spheroid (e.g. in- or circum-scribed around the hexagonal crystal) would not have the same volume, and are therefore unphysical.

Senior (1976) shows that these normalised values for X_{ii} should be bounded from below by $(\epsilon - 1)/\epsilon = 0.68$, and indeed all the numerical data does satisfy this condition. We also note that X_{zz} approaches this limit for thin plates (data point at $w = 100$). For long slender columns ($w \ll 1$), and very thin plates ($w \gg 1$), the Gans (1912) spheroid theory

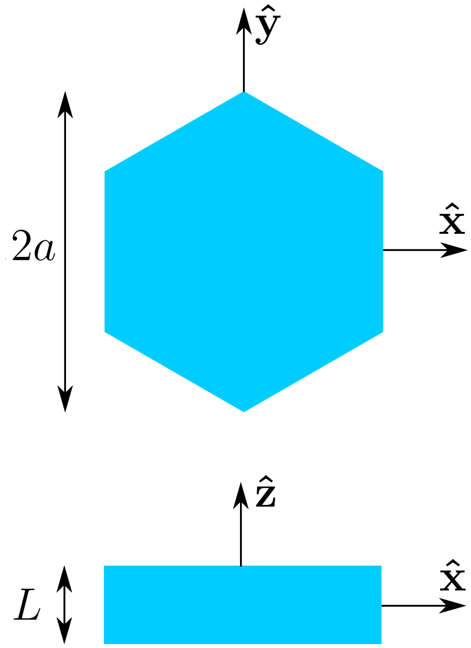

Figure 1. Schematic showing the orientation of a hexagonal prism crystal relative to the basis vectors $\hat{\mathbf{x}}$, $\hat{\mathbf{y}}$ and $\hat{\mathbf{z}}$, seen from two orthogonal viewpoints. Also indicated is the length of the crystal L and width $2a$.

gives results which are very close to the hexagonal prism calculations, indicating that in these limits the spheroidal approximation is an accurate one. However, for less extreme aspect ratios there are significant discrepancies. One of the most obvious features of figure 2 is that the point where the polarisability along both axes are equal ($X_{xx} = X_{zz}$) is significantly shifted in the DDA results ($w \approx 1.3$) relative to the spheroid prediction ($w = 1$). For plate crystals the spheroid model predicts a polarisability along the $\hat{\mathbf{z}}$ axis which is too small, and a polarisability in the $\hat{\mathbf{x}}$-$\hat{\mathbf{y}}$ plane which is too large.

For example, consider a plate with $w = 3$. The spheroidal approximation predicts a value which is 12% too low for X_{zz}, and 5% too high for X_{xx} and X_{yy}. These may appear to be relatively modest errors, but note that equation 3 means that the radar cross-section is proportional to the square of these polarisabilities. For horizontally oriented hexagonal plates probed by a radar dwelling at horizontal equations 8 and 9 tell us that $\sigma_{\mathrm{co,h}}$ will be 10% too large, while $\sigma_{\mathrm{co,v}}$ will be 25% too small, and this means that the spheroidal assumption leads to a 38% (1.5dB) overestimate in Z_{DR}. This is a significant error.

The impact on the specific differential phase shift K_{DP} is smaller than for differential reflectivity because it is proportional to $X_{xx} - X_{zz}$ (Oguchi 1983). For our oriented plate therefore we should expect a 17% overestimate in the computed K_{DP} using the spheroid approximation. Although smaller than the error in Z_{DR}, this is not a negligible error in the author's opinion.

Figure 3 shows calculations of Z_{DR} for horizontally oriented plate and column crystals as a function of aspect ratio, using both the DDA data for hexagonal plates, and the theoretical curves for spheroids. The spheroid calculations in figure 3 are identical to those of Hogan *et al.* (2002) except we have assumed that the change in orientation between plates and columns occurs not at an aspect ratio of $w = 1$, but at $w = 1.1$ based on the laboratory experiments of Westbrook (2011). His data show that columns and

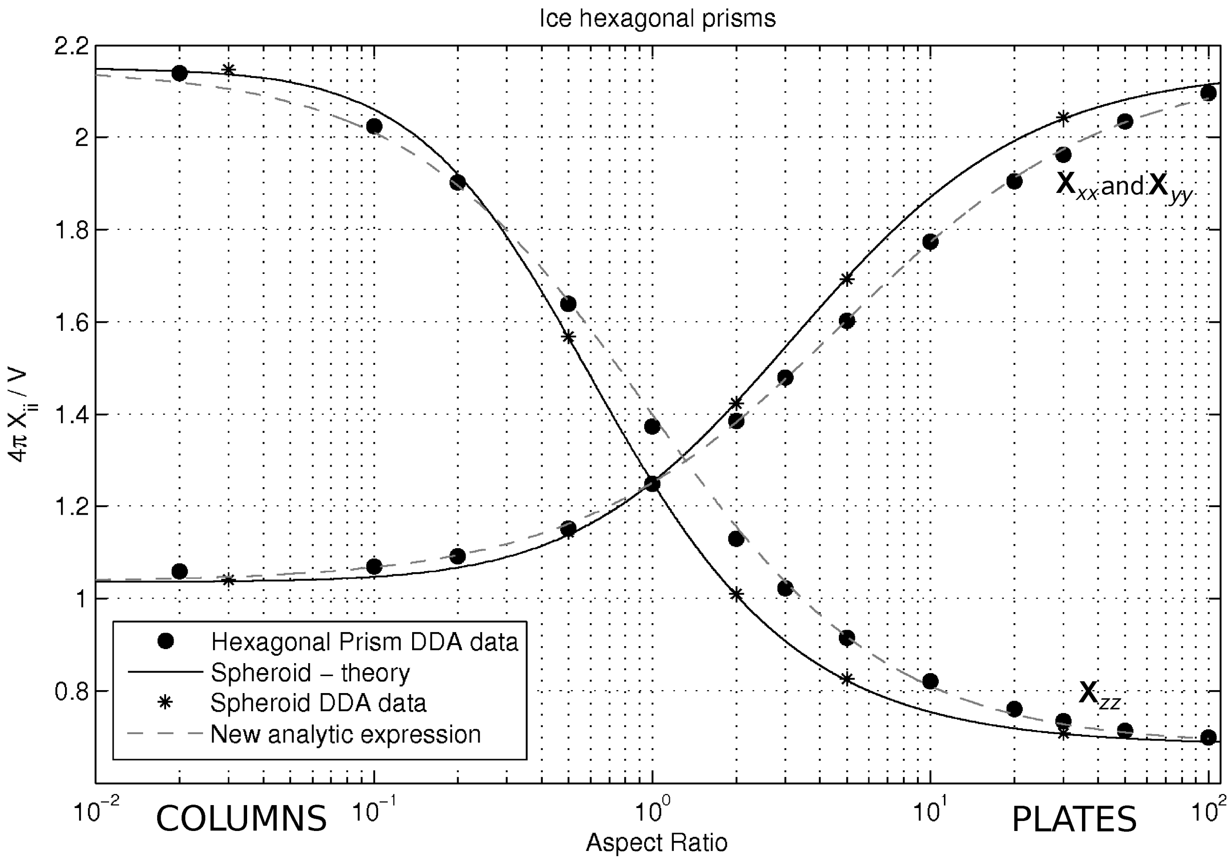

Figure 2. DDA calculations of the polarisability tensor elements X_{xx} and X_{zz} (circles) for hexagonal prisms. Also shown are theoretical curves for spheroids (black solid curve), DDA results for spheroids (asterisks) and the new empirical formula for hexagonal prisms described in the text (grey dashed line).

thick plates with $w < 1.1$ are oriented with their $\hat{\mathbf{z}}$ axis horizontal, while plates with $w > 1.1$ have their $\hat{\mathbf{z}}$ axis vertical. This assumption leads to a slight discontinuity in the theoretical spheroid curve at $w = 1.1$ since this cross-over in orientation no longer coincides with the point where $X_{xx} = X_{zz}$ ($w = 1$ for spheroids), and means that there is a narrow region of parameter space between $w = 1$ and 1.1 (thick plates) where Z_{DR} is predicted to be slightly negative (-0.2dB at $w = 1.1$).

For plates of all aspect ratios we observe that the spheroidal approximation systematically overestimates the magnitude of Z_{DR}. This is most pronounced for aspect ratios between 1.1 and 10 where Z_{DR} is 1—1.5dB too large; for a more extreme aspect ratio of 100 the error is reduced to only 0.2dB. For column crystals the spheroid approximation is more accurate: errors are 0.5dB or less in general.

The differences between hexagonal crystals and their spheroid ‘equivalents’ appears to be significant for polarimetric radar applications. However, it is important to establish that this a genuine effect, and not a numerical artefact. To this end some test DDA calculations were performed. Identical dipole volume element spacings were used to the hexagonal plate computations, but instead of hexagonal crystals, spheroidal particles were generated, and their polarisability tensor elements computed. The results of these computations at aspect ratios of 0.03, 0.5, 2, 5 and 30 are shown by the asterisk markers in figure 2. The calculations are in excellent agreement with the theoretical curves for spheroids. This gives us confidence that our DDA calculations are accurate, and that the discrepancy between our hexagonal results and the Gans (1912) spheroidal model is genuine.

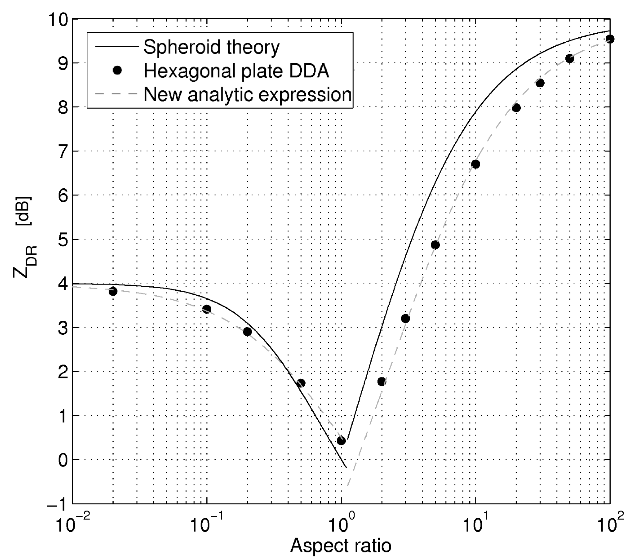

Figure 3. Differential reflectivity predicted for horizontally oriented hexagonal plate crystals of various aspect ratios viewed at horizontal incidence (circles). Also shown are theoretical results for spheroid model (solid black line) and the new empirical formula for hexagonal prisms described in the text (grey dashed line).

3.2. Empirical modification of the Gans equations: new analytical expressions

Based on the results above the spheroidal model is not an accurate representation of hexagonal ice crystals and it would be desireable to replace it or modify it in order to improve the accuracy of scattering calculations without needing to recompute the polarisability tensor for each possible aspect ratio. Based on the observation that $X_{xx} \approx X_{yy}$, and that the spheroidal polarisabilities in figure 2 have a qualitatively similar shape to our DDA data, we start by assuming that our polarisability tensor elements will have the same functional form (equation 5) as spheroids, but with different geometrical factors L_i. Under this assumption, we can compute $L_x = L_y$ and L_z from our DDA data by inverting equation 5. Given that we observe in figure 2 than the asymptotic limits seem to be the same as for spheroids, we expect that for thin plates $L_x \to 0$ and $L_z \to 1$, whilst for long slender columns $L_x \to \frac{1}{2}$ and $L_z \to 0$ (van de Hulst 1957). Using these limits, two simple functions with the correct asymptotic limits were fitted to the numerical data for $L_x = L_y$ and L_z:

$$L_z = \frac{1}{2}\left(\frac{1-3/w}{1+3/w}+1\right) \quad (12)$$

$$L_x = L_y = \frac{1}{4}\left(\frac{1-0.5w^{0.9}}{1+0.5w^{0.9}}+1\right) \quad (13)$$

where $w = (2a/L)$ is the aspect ratio. Unlike spheroids these formulae (and our numerical data) do not satisfy $L_x + L_y + L_z = 1$.

Applying these new equations to compute $\mathbf{X}$ yields the grey dashed lines in figure 2, which is an excellent approximation to the numerical data, with RMS errors of 1% and 0.5% respectively for X_{zz} and X_{xx}.

Applying this curve to the computation of Z_{DR} leads to the grey dashed curve in figure 3, again providing a very close approximation to the numerical data to within a tenth of a dB. As for spheroids we observe a slight discontinuity at $w = 1.1$ because the cross-over in the orientation of the crystals at $w = 1.1$ does not coincide with the point where $X_{xx} = X_{zz}$ at $w \approx 1.3$, and again small negative differential reflectivities of up to -0.6dB are theoretically possible in the narrow region of parameter space between these two aspect ratios.

It is noteworthy that equations 12 and 13 are in fact simpler than the exact expressions for spheroids. They are also easier to apply because no split into prolates and oblates is necessary, and there are no numerical difficulties in the case of $w = 1$ (unlike equations 7 and 6).

3.2.1. Testing the new analytical expression for smaller permittivities

Thus far we have assumed that the elements X_{ii} take the form given in equation 5. To test this assumption, a number of DDA calculations have been made where the relative permittivity has been reduced relative to the value for solid ice, while the geometry remained fixed ($w = 10$ in the data presented here). This will allow us to test whether the assumed separation of the permittivity and shape dependency in equation 5 is in fact the correct one. A motivation for this is that we would like to be able to use our new expression to predict the scattering from more complex pristine crystals such as branched hexagonal plates (stellar and dendritic crystals), and one way to approach this problem is to treat the more complex particle as a hexagonal prism of the same overall dimensions, but with a reduced permittivity based on the fraction of the prism which is composed of ice. This will be discussed in section 4.

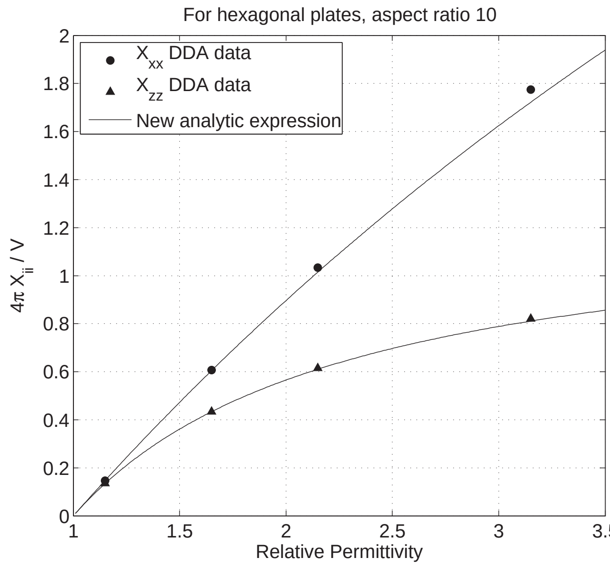

Figure 4. DDA calculations of the polarisability tensor elements X_{xx} and X_{zz} for hexagonal plates with reduced permittivities (markers). Solid lines show prediction using the new model.

Figure 4 shows the resulting normalised polarisability tensor elements where the real part of the permittivity is 3.15 (the value for solid ice), 2.15, 1.65 and 1.15. Also shown in the figure (solid lines) are the predicted values, based on equations 5, 12, 13. The new equations are indistinguishable from the numerical data, indicating that the separation of the geometry and permittivity factors in equation 5 is the correct one, at least for these relatively weak permittivity values.

3.2.2. Effect of crystal fluttering on Z_{DR} errors

In section 3.1 we considered the error in calculations of Z_{DR} when approximating a horizontally oriented hexagonal crystal with a horizontally oriented spheroid. Westbrook *et al.* (2010) showed that such crystals are frequent in mid-level mixed-phase layer clouds. However large hexagonal ice crystals (with Reynolds number ~ 100 or greater) do not have a perfectly horizontal orientation, but fall unsteadily (Kajikawa 1992), leading to a distribution of orientations relative to the fixed polarisation of the radar. To investigate whether the spheroid approximation also leads to similar errors in the case of unsteady fall, Z_{DR} was computed for an ensemble of ice crystals, each rotated by an angle ϕ, where ϕ was sampled from a uniform distribution of angles in the range $\pm\phi_{\max}$. To calculate σ_{co} from these rotated crystals, one simply needs to ensure that $\hat{\mathbf{E}}_0$ is defined correctly relative to the $\hat{\mathbf{x}}, \hat{\mathbf{y}}, \hat{\mathbf{z}}$ basis vectors of $\mathbf{X}$ when applying equation 3. A detailed discussion of this is provided by Russchenberg (1992) and Bringi and Chandrasekar (2001). Since the most significant errors in figure 3 were for hexagonal plates, we focus on these particles here, and figure 5 shows the difference between the Z_{DR} computed using

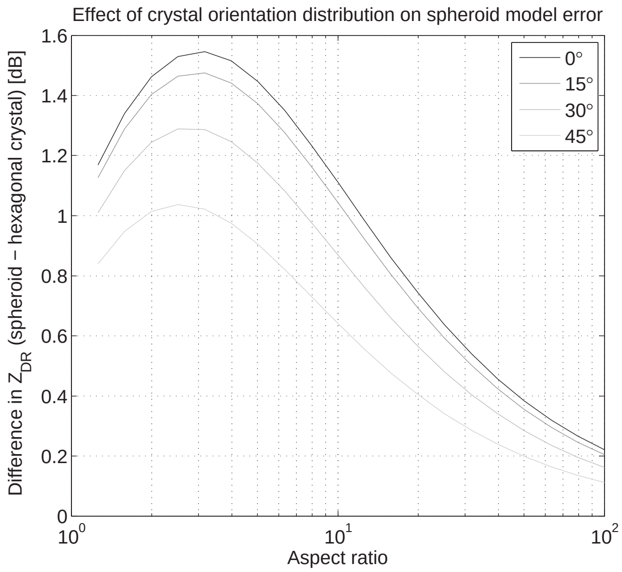

Figure 5. Error in differential reflectivity of hexagonal plate crystals when computed using the Gans spheroid model, as a function of aspect ratio and the distribution of fluttering angles assumed (see text). Different lines show maximum fluttering angles of $\phi_{\max} = 0$, 15, 30 and 45°.

spheroids, and the Z_{DR} computed using the new results for hexagonal crystals. For $\phi_{\max} = 15°$ the error associated with approximating plates as spheroids is almost identical to the case of perfect horizontal orientation ($\phi_{\max} = 0°$), to within 0.1dB. As the distribution of crystal orientations becomes broader, the error in approximating the crystals as spheroids becomes gradually smaller: for example at $w = 2$ the error is 1.45 dB for $\phi_{\max} = 0°$, falling to 1 dB for $\phi_{\max} = 45°$. These results suggest that even for rather broad distributions of crystal fall orientation, the error in Z_{DR} from approximating hexagonal crystals as spheroids can be significant.

4. Broad-branched, stellar and dendritic ice crystals

Plate crystals formed at high supersaturations often grow preferentially at the corners and develop branches, leading to broad-branched, stellar and dendritic crystal types (Takahashi *et al.* 1991). The polarisability tensor was computed in the same manner as before for a number of idealised branched crystal geometries. The geometries of the crystals follows those considered in Westbrook *et al.* (2008).

We first consider stellar and broad-branched crystals. The specific model geometries used here are shown in cross-section in figure 6a; in all cases the aspect ratio was $w = 10$. Again, the hexagonal symmetry means that the polarisability tensor is diagonal. The elements of $\mathbf{X}$ were computed using DDA as before. As for hexagonal prisms we again observe from the numerical data that $X_{xx} = X_{yy}$. The results for X_{xx} and X_{zz} are plotted in figure 7 (filled markers) as a function of the volume fraction f which we define here as the volume of ice in the crystal, divided by the volume V of a hexagonal prism of the same span and length. As in section 3 the results have been normalised by a factor $V/(4\pi)$. Both X_{xx} and X_{zz} decrease monotonically with decreasing volume fraction as one moves from broad-branch crystals with $f = 0.96$ down to tenuous star-shaped crystals with $f = 0.11$. This is

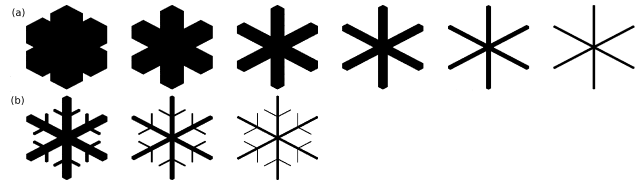

Figure 6. Branched crystal shapes used in DDA calculations. Panel (a) shows the broad-branched and stellar crystal shapes simulated in section 4 as a cross-section in the $\hat{\mathbf{x}}$–$\hat{\mathbf{y}}$ plane. Similarly panel (b) shows more complex branched dendritic examples included in section 4.

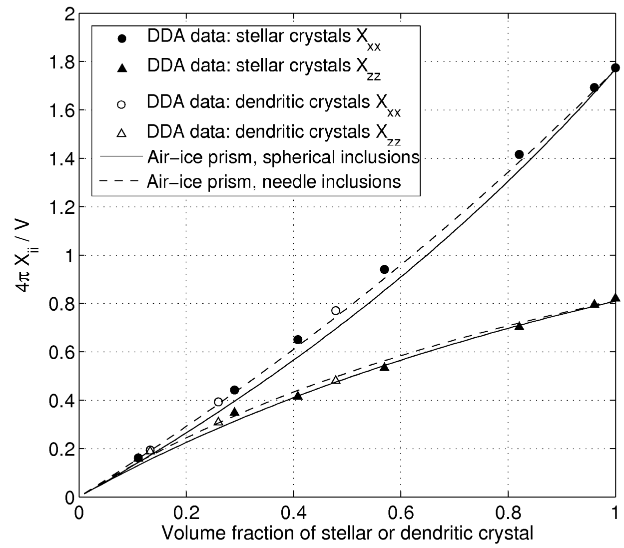

Figure 7. DDA calculations of the polarisability tensor elements X_{xx} and X_{zz} for stellar and dendritic crystals as a function of ice volume fraction relative to a solid hexagonal plate of the same span. Solid and dashed lines show results obtained using a simple air-ice hexagonal prism using the Maxwell-Garnett mixture theory for spherical and needle-shaped inclusions respectively.

physically sensible, since as f becomes smaller the volume of ice in the particle is smaller, and hence less scattering can occur. More importantly, we note that the curves for X_{xx} and X_{zz} converge as $f \to 0$ this means that for tenuous particles polarisation effects become steadily weaker, a result anticipated by Bader *et al.* (1987).

More complicated dendritic crystal shapes, shown in figure 6b were also simulated using DDA. The results of these computations is also shown in figure 7 (open markers). The results appear to follow the same behaviour as the simpler branched crystals, with decreasing volume fraction (spanning the range 0.48 to 0.13) corresponding to a decrease in the polarisability of the particles and a convergence of the two polarisability tensor elements.

Since there seems to be a rather well-defined dependence of the change in the polarisabilities of the crystal as a function of the volume fraction, it suggests that the scattering from these more complex particles can be characterised by the dipole moments of an enclosing hexagonal prism and the volume fraction f. One way to do this would be to simply fit a curve to the numerical data in figure 7. Perhaps a more physically satisfactory approach is to use a dielectric mixture theory to represent the complex particle as a solid hexagonal prism with a reduced permittivity. The essence of these mixture theories is that the complexities of the particle (i.e. the branches of the dendrite surrounded by air) are approximated by a homogeneous mixture of air and ice with an effective permittivity which lies somewhere between the two ($\epsilon = 1$—3.15). A detailed overview of dielectric mixture theory is provided by Sihvola (1989). Obviously this is a relatively crude approximation to the complex geometry of the ice crystals: however as we will see, it appears to be an acceptable one for these crystals. The most common of these theories is attributed to Maxwell-Garnett (1904) and prescribes the effective permittivity as:

$$\epsilon_{\text{eff}} = \frac{(1-f) + f\beta\epsilon}{1 - f + f\beta} \tag{14}$$

Bohren and Huffman (1983) has shown that Maxwell-Garnett's original approximation can be generalised depending upon the shape of the ice 'inclusions' in the mixture. For spherical inclusions the paramater $\beta = 3/(\epsilon + 2) = 0.58$. For randomly oriented rod-shaped inclusions $\beta = 0.65$.

We can use equation 14 in addition to the new equations for hexagonal prisms developed in section 3 to calculate the polarisability tensor elements for the branched crystals. The results of this calculation are shown by the solid line (spherical inclusions) and dashed line (rod-shaped inclusions) in figure 7. Both estimates capture the behaviour of the numerical data well, although assuming rod inclusions appears to be slightly more accurate. For $f \sim 0.5$ the spherical Maxwell-Garnett curve underestimates $\mathbf{X}_{xx}$ by about 10%, whilst for rod-inclusions the differences are typically $\approx$ 2%. One may speculate that the branches of the crystals are not entirely dissimilar to rod shapes oriented in many different angles, and this may be the reason for the better agreement with that theory.

5. Conclusions

In this note we have shown that modelling hexagonal ice crystals as spheroids may lead to significant error in calculations of dual-polarisation measurements such as differential reflectivity. It was shown that hexagonal crystals, like spheroids can be characterised by only two elements of the polarisability tensor $\mathbf{X}$. These elements could be accurately captured by making a simple modification of the geometrical factors L_i used in Gans's theory for spheroids, and the resulting formulae are in fact simpler to apply in practice as well as more accurate. It is therefore recommended that future polarimetric studies which seek to model the scattering from oriented crystals use the new expression developed here.

A key advantage of setting the numerical DDA results in the polarisability tensor framework of Senior (1976) is that we can deterimne the scattering properties for a crystal of any desired volume, in any desired orientation relative to the polarisation of the applied wave. The proposed modification of the Gans equations takes this generalisation further to allow calculations for any desired aspect ratio, or permittivity between 1 and 3.15 to be rapidly performed. The scattered field can be determined in the forward (or indeed an arbitrarily chosen) scattering direction, in addition to backscatter, allowing one to predict propagation effects such as specific differential phase shift.

DDA calculations of more complex branched crystals show that they can be accurately approximated by a hexagonal prism of the same length and width, but with a reduced permittivity prescribed by Maxwell-Garnett theory, allowing a rather simple interpretation of the scattering properties in terms of the aspect ratio and volume fraction.

Acknowledgement

I am grateful to BT Draine and PJ Flatau for making their discrete dipole approximation computer package DDSCAT freely available: all of the DDA calculations presented here were performed using this package. I am also grateful to the IT support staff in the Department of Meteorology for their help in compiling DDSCAT version 7.3, and to two anonymous reviewers for their constructive comments.

References

Andrič J, Kumjian MR, Zrnić DS, Straka JM and Melnikov VM 2013. Polarimetric Signatures above the Melting Layer in Winter Storms: An Observational and Modeling Study *J. Appl. Meteorol. & Climatol.* **52** 682–700.

Atlas D and Ludlam FH 1961. Multi-wavelength radar reflectivity of hailstorms. *Q. J. R. Meteorol. Soc.* **87** 523–534

Bader MJ, Clough SA and Cox GP 1987. Aircraft and dual polarization radar observations of hydrometeors in light stratiform precipitation. *Q. J. R. Meteorol. Soc.* **113** 491–515

Bohren CF and Huffman DR 1983. *Absorption and scattering of light by small particles* Wiley, New York.

Bringi VN and Chandrasekar V 2001. *Polarimetric Doppler weather radar* Cambridge University Press.

Draine BT and Flatau PJ 1994. Discrete dipole approximation for scattering calculations *J. Optic. Soc. Amer. A* **11** 1491–1499.

Evans KF and Vivekanandan J 1990. Multiparameter Radar and Microwave Radiative Transfer Modeling of Nonspherical Atmospheric Ice Particles *IEEE Trans. Geosci. & Rem. Sens.* **28** 423–436

Gans R 1912. Über die Form ultramikroskopischer Goldteilchen *Ann. Phys.* **37** 881–900.

Hall MPM, Goddard JW and Cherry SM 1984. Identification of hydrometeors and other targets by dual-polarisation radar *Radio Sci.* **19** 132–140.

Heymsfield AJ and Knollenberg RG 1972. Properties of Cirrus Generating Cells *J. Atmos. Sci.* **29** 1358–1366.

Hogan RJ, Field PR, Illingworth AJ, Cotton RJ and Choularton TW 2002. Properties of embedded convection in warm-frontal mixed-phase cloud from aircraft and polarimetric radar *Q. J. R. Meteorol. Soc.* **128** 451–476.

Illingworth AJ 2003. Improved Precipitation rates and data quality by using polarimetric measurements in *Advanced Applications of Weather Radar* Springer.

Kajikawa M 1992. Observations of the falling motion of plate-like snow crystals part I: the free-fall patterns and velocity variations of unrimed crystals *J. Meteorol. Soc. Jap.* **70** 1–8.

Liebe HJ, Manabe T and Hufford GA 1989. Millimeter-wave attenuation and delay rates due to fog/cloud conditions *IEEE Trans. Ant. & Prop.* **37** 1617–1623.

Liu G 2008. A Database of Microwave Single-Scattering Properties for Nonspherical Ice Particles *Bull. Amer. Meteorol. Soc.* **89** 1563–1570.

Maxwell-Garnett JC 1904. Colours in metal glasses and metallic films *Philos. Trans. Roy. Soc. London* **A203** 385–420.

O'Brien SG and Goedecke GH 1988. Scattering of millimeter waves by snow crystals and equivalent homogeneous symmetric particles *Appl. Opt.* **27** 2439–2444

Oguchi T 1983. Electromagnetic wave propagation and scattering in rain and other hydrometeors *Proc. IEEE* **71** 1029–1078.

Pruppacher H and Klett JD 1997. *Microphysics of clouds and precipitation* second edition, Kluwer.

Russchenberg H 1992. *Ground-based remote sensing of precipitation using a multi-polarized FM-CW Doppler radar* PhD thesis, Delft University Press.

Ryzhkov AV, Zrnic DS and Gordon BA 1998. Polarimetric Method for Ice Water Content Determination *J. Appl. Meteorol.* **37** 125–134.

Ryzhkov AV, Schuur TJ, Burgess DW, Heinselman PL, Giangrande SE and Zrnić DS 2005. The Joint Polarization Experiment: Polarimetric

Rainfall Measurements and Hydrometeor Classification *Bull. Amer. Meteorol. Soc.* **89** 809–824.

Schneider TL and Stephens GL 1995. Theoretical Aspects of Modeling Backscattering by Cirrus Ice Particles at Millimeter Wavelengths *J. Atmos. Sci.* **52** 4367–4385

Seliga TA and Bringi VN 1976. Potential Use of Radar Differential Reflectivity Measurements at Orthogonal Polarizations for Measuring Precipitation *J. Appl. Meteorol.* **15** 69–76.

Senior TBA 1976. Low-frequency scattering by a dielectric body *Radio Sci.* **11** 477–482.

Sihvola AH 1989. Self-consistency aspects of dielectric mixture theories *IEEE Trans. Geosci. & Rem. Sens.* **27** 403–415.

Takahashi T, Endoh T and Wakahama G 1991. Vapor diffusional growth of free-falling snow crystals between -3 and $-23°$C *J. Meteorol. Soc. Jap.* **69** 15–30.

van de Hulst HC 1957. *Light scattering by small particles* Chapman and Hall, London.

Westbrook CD, Hogan RJ and Illingworth AJ 2008. The Capacitance of Pristine Ice Crystals and Aggregate Snowflakes *J. Atmos. Sci.* **65** 206–219.

Westbrook CD, Illingworth AJ, O'Connor EJ and Hogan RJ 2010. Doppler lidar measurements of oriented planar ice crystals falling from supercooled and glaciated cloud layers *Q. J. R. Meteorol. Soc.* **136** 260–276.

Westbrook CD 2011. Origin of the Parry arc *Q. J. R. Meteorol. Soc.* **137** 538–543.

Westbrook CD and Illingworth AJ 2013. The formation of ice in a long-lived supercooled layer cloud *Q. J. R. Meteorol. Soc.* in press DOI: 10.1002/qj.2096

Zubko E Petrov D, Grynko Y, Shkuratov Y, Okamoto H, Muinonen K, Nousiainen T, Kimura H, Yamamoto T, and Videen G 2010. Validity criteria of the discrete dipole approximation *Appl. Opt.* **49** 1267–1279.